Wetting behavior of CaO–Al$_2$O$_3$-based mold flux with various BaO and MgO contents on the steel substrate

Lejun Zhou, Hao Luo, Wanlin Wang, Houfa Wu, Erzhuo Gao, You Zhou, and Daoyuan Huang

Articles you may be interested in

Ying Xu, Zhi-peng Yuan, Li-guang Zhu, Yi-hua Han, and Xing-juan Wang, Shear-thinning behavior of the CaO-SiO$_2$-CaF$_2$-Si$_3$N$_4$ system mold flux and its practical application, *Int. J. Miner. Metall. Mater.*, 24(2017), No. 10, pp. 1096-1103. https://doi.org/10.1007/s12613-017-1500-8

Bo Zhang, Wen Li, Hong Li, and Hai-feng Zhang, Spontaneous infiltration and wetting behaviors of a Zr-based alloy melt on a porous SiC substrate, *Int. J. Miner. Metall. Mater.*, 25(2018), No. 7, pp. 817-823. https://doi.org/10.1007/s12613-018-1630-7

Jing Guo, Shu-sen Cheng, Han-jie Guo, and Ya-guang Mei, Novel mechanism for the modification of Al$_2$O$_3$-based inclusions in ultra-low carbon Al-killed steel considering the effects of magnesium and calcium, *Int. J. Miner. Metall. Mater.*, 25(2018), No. 3, pp. 280-287. https://doi.org/10.1007/s12613-018-1571-1

Ze-yun Cai, Bo Song, Long-fei Li, Zhen Liu, and Xiao-kang Cui, Effect of CeO$_2$ on heat transfer and crystallization behavior of rare earth alloy steel mold fluxes, *Int. J. Miner. Metall. Mater.*, 26(2019), No. 5, pp. 565-572. https://doi.org/10.1007/s12613-019-1765-1

Peng Fei, Yi Min, Cheng-jun Liu, and Mao-fa Jiang, Effect of continuous casting speed on mold surface flow and the related near-surface distribution of non-metallic inclusions, *Int. J. Miner. Metall. Mater.*, 26(2019), No. 2, pp. 186-193. https://doi.org/10.1007/s12613-019-1723-y

Tao Zhang, Jian Yang, Gang-jun Xu, Hong-jun Liu, Jun-jun Zhou, and Wei Qin, Effects of operating parameters on the flow field in slab continuous casting molds with narrow widths, *Int. J. Miner. Metall. Mater.*, 28(2021), No. 2, pp. 238-248. https://doi.org/10.1007/s12613-020-1988-1

IJMMM WeChat   QQ author group

Wetting behavior of CaO–Al$_2$O$_3$-based mold flux with various BaO and MgO contents on the steel substrate

Lejun Zhou[1,2], *Hao Luo*[1,2], *Wanlin Wang*[1,2,✉], *Houfa Wu*[1,2], *Erzhuo Gao*[1,2], *You Zhou*[1,2], *and Daoyuan Huang*[1,2]

1) School of Metallurgy and Environment, Central South University, Changsha 410083, China
2) National Center for International Cooperation of Clean Metallurgy, Changsha 410083, China

Abstract: The interfacial phenomena in mold have a great impact on the smooth operation of continuous casting process and the quality of the casting product. In this paper, the wetting behavior of CaO–Al$_2$O$_3$-based mold flux with different BaO and MgO contents was studied. The results showed that the contact angle between molten flux and interstitial free (IF) steel substrate increased from 62.4° to 74.5° with the increase of BaO content from 3wt% to 7wt%, while it decreased from 62.4° to 51.3° with the increase of MgO content from 3wt% to 7wt%. The interfacial tension also increased from 1630.3 to 1740.8 mN/m when the BaO content increased, but it reduced from 1630.3 to 1539.7 mN/m with the addition of MgO. The changes of contact angle and interfacial tension were mainly due to the fact that the bridging oxygen (O^0) at the interface was broken into non-bridging oxygen (O$^-$) and free oxygen (O^{2-}) by MgO. However, more O$^-$ and O^{2-} connected into O^0 when BaO was added, since the charge compensation effect of BaO was so stronger that it offset the effect of providing O^{2-}.

Keywords: mold flux; wetting; contact angle; interfacial tension; melt structure; continuous casting

1. Introduction

CaO–Al$_2$O$_3$-based mold flux has become a potential function material for the continuous casting process of the high aluminum steel, since it can reduce the chemical reaction between the active alloy, Al, in molten steel and the component, i.e., SiO$_2$, in mold flux, and then stabilizes its performances [1–2]. When the CaO–Al$_2$O$_3$-based mold flux is added into mold, it works as very important roles to protect the molten steel from oxidation, insulate the heat loss, assimilate the inclusions, lubricate the shell, and control the horizontal heat transfer in mold [3]. However, continuous casting mold is also a high temperature container with multiphase coexistence, such as molten steel, molten flux, solidified shell, mold wall, un-melted flux, inclusions, and bubbles. The interfacial phenomena occurring among those phases have the great impacts on slag entrapment [4], nozzle erosion [5], bubble capture [6–7], slag rim formation [8], etc., consequently affect the smooth operation of the continuous casting process and the quality of the casting product.

The interfacial properties between mold flux and steel have been investigated by many researchers. Sharan and Cramb [9] studied the effect of oxygen on the surface tension of Fe–Ni alloys, they found that oxygen is an extremely surface active in both molten Fe and Fe–Ni alloy. Lee and Morita [10] focused their research on the evaluation of surface tension for liquid Fe–S alloys, the result showed that the surface tension also decreases greatly with the increase of sulfur contents. So, these non-metallic elements, such as O and S, are of surface actives for molten Fe. As for metallic elements, Nakashima and Mori [11] summarized the variations of interfacial tension between the liquid iron alloys and liquid slags based on a lot of previous works, they believed that the addition of most of alloy elements, including Ni, Ti, Mn, Mo, V, etc., can reduce the interfacial tension except tungsten (W). Jung *et al*. [12] investigated the interfacial tension between solid iron and CaO–SiO$_2$–MO (M = Fe, Mn) system, results indicated a decrease in the interfacial tension with the additions of amphoteric oxide.

Although significant works related to the interfacial properties have been conducted, most of them concerned on iron or steel. Very few of them considered the effect of composition of slag, especially composition of the CaO–Al$_2$O$_3$-based mold flux, on the interfacial properties between molten flux and steel. Therefore, in this study, the wetting behavior of CaO–Al$_2$O$_3$-based mold flux with different BaO and MgO contents was carried out using the sessile drop method. The contact angle between the molten flux and the IF steel substrate was measured, and the interfacial tension was also calculated. In addition, the oxygen species at the flux/steel interface were also determined using XPS to demonstrate the intrinsic connections between mold flux compositions, interfa-

🖄 Springer

cial properties and melt structure.

2. Experimental

2.1. Sample preparation

The CaO–Al$_2$O$_3$-based mold flux samples in this experiment were made from pure chemical reagents, such as CaCO$_3$, SiO$_2$, Al$_2$O$_3$, Na$_2$CO$_3$, Li$_2$CO$_3$, CaF$_2$, BaCO$_3$, and MgO. The compositions of the mold fluxes are listed in Table 1. Among these fluxes, Samples 1–3 were designed by the addition of 3wt%, 5wt%, and 7wt% BaO, respectively, and with a (CaO+BaO)/Al$_2$O$_3$ mass ratio (C/A) of 1.5. Samples 1, 4, and 5 were designed by the variation of MgO content from 3wt% and 5wt% to 7wt%, respectively. There are two reasons why BaO and MgO were concerned here. One is that it is hopeful to use BaO as a substitution for CaO, and then reduces the negative effects caused by the too high basicity in mold flux. The other is that magnesia is a common component of refractory materials, the erosion of those refractory materials can result in an increase of MgO in mold flux due to the capture of MgO contained inclusions.

During the flux samples preparation, all the reagents were dried in a drying oven at the temperature of 423 K for 1 h to ensure the accuracy of weighing. Then, they were melted in an induction furnace at 1773 K for 15 min to homogenize their compositions. The molten fluxes were poured onto a water-cooled copper plate to obtain solid glassy fluxes. At last, the flux samples for the sessile drop experiment were obtained by polishing these glassy fluxes into small cubes with a side length of 5 mm. The chemical compositions of pre-melted sample in Table 1 are designed compositions, while the chemical compositions of the post-melted mold fluxes were also analyzed using the inductively coupled plasma optical emission spectroscopy (ICP-OED; Spectroblue, Spectro Corporation, Germany), X-ray fluorescence (XRF; S4 Pioneer, Bruker AXS, Karlsruhe, Germany), and the ion-selective electrode method (ISE; PF-2-01, Shanghai LEICI Corporation, China). The results suggest that the volatilization loss of components in the mold fluxes can be ignored since the changes of the compositions were very small, as listed in Table 1.

The substrates used in this experiment were made of IF steel (interstitial free steel). Table 2 shows major chemical composition of the IF steel. These substrates were made by cutting the steel into small sheets with a size of 30 mm × 30 mm × 3 mm. The sheets also were ground and polished by SiC sandpapers with a grit size down to 2000 to control their surface roughness.

Table 1.   Chemical compositions of the pre- and post-melted mold fluxes   wt%

Condition	Sample	C/A	CaO	SiO$_2$	Al$_2$O$_3$	Na$_2$O	Li$_2$O	F	BaO	MgO
	1	1.5	39.0	7.0	28.0	10.0	3.0	7.0	3.0	3.0
	2	1.5	37.0	7.0	28.0	10.0	3.0	7.0	5.0	3.0
Pre-melted	3	1.5	35.0	7.0	28.0	10.0	3.0	7.0	7.0	3.0
	4	1.5	37.8	7.0	27.2	10.0	3.0	7.0	3.0	5.0
	5	1.5	36.6	7.0	26.4	10.0	3.0	7.0	3.0	7.0
	1	1.51	38.91	7.01	27.76	10.13	2.95	6.93	2.97	3.03
	2	1.47	36.13	6.86	27.89	10.19	2.98	6.91	4.95	3.05
Post-melted	3	1.46	33.62	7.17	27.68	10.03	3.03	6.96	6.86	2.99
	4	1.49	37.56	7.09	27.18	10.02	2.99	6.98	2.98	4.89
	5	1.50	36.69	6.92	26.53	10.14	2.97	6.87	3.06	6.96

Table 2.   Major chemical composition of IF steel   wt%

C	Si	Mn	Al	Ti	N	O
0.0007–0.0020	0.0011–0.0065	0.0950–0.1350	0.0150–0.0685	0.0250–0.0750	0.0012–0.0016	0.0006–0.0009

2.2. Sessile drop test

The wetting behavior of CaO–Al$_2$O$_3$-based mold flux on the IF steel substrate was tested by the sessile drop method. The schematic figure of the apparatus is shown in Fig. 1 [13]. It is mainly composed of a horizontal furnace with MoSi$_2$ heating elements, an image acquisition system, an atmosphere control system, and a temperature control system.

The cubic mold flux sample was placed on the middle of the IF steel sheet as shown in Fig. 2, and then pushed into the horizontal heating furnace. The furnace was evacuated to 0.1 MPa by a vacuum pump after sealing both ends of the furnace tube. High-purity (99.999%) Ar gas was introduced into the furnace tube with a flow rate of 200 mL/min through a gas purification device. The gas purification device was

filled with Mg, Al, Ti, and Cu getters, and it was heated to the temperature of 673 K [14]. Only in this way, the oxygen partial pressure in the furnace could be controlled at 10^{-15} Pa.

The furnace, together with the samples, was heated up to 1773 K at a heating rate of 5 K/min (5°C/min), and then kept at that temperature for 30 min. The entire experiment process was recorded by a high-resolution charge coupled device (CCD) digital camera with a filter placed at one end of the furnace. The wetting behavior and change of contact angle were observed and analyzed by the camera and Image-J software.

2.3. XPS analysis

To study the effect of melt structure of the CaO–Al$_2$O$_3$-based mold flux on the interfacial properties of flux and steel,
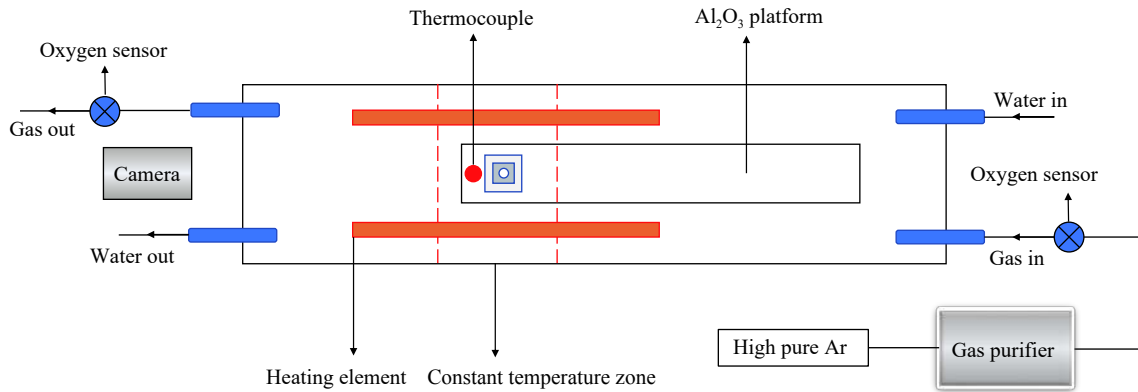
Fig. 1.   Schematic figure of the sessile drop method. Redrew by permission from Springer Nature: *Met. Mater. Int.*, **Effect of MnO content on the interfacial property of mold flux and steel, W.L. Wang, J.W. Li, L.J. Zhou, and J. Yang, Copyright 2010.**
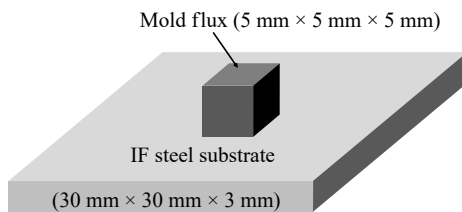

Fig. 2.   Schematic figure of the mold flux and substrate samples.

the flux samples after the sessile drop test were carefully stripped off from the steel substrates. The stripped flux samples were further etched by an Ar ion beam for 30 min to clear the surface contamination, and then analyzed by X-ray photoelectron spectroscopy (XPS; PHI-5300/ESCA, PerkinElmer Corporation, USA). The XPS analysis was conducted through an X-ray photoelectron spectrometer at 3.0 kV/25 mA with an Al/Mg K$_\alpha$ X-ray source. The results were calibrated by the C 1s binding energy at 284.8 eV. In addi-

tion, Origin Microcal Software (OriginPro 9.0) was used to deconvolute the XPS spectra to gain the fraction of each oxygen ion species as previous papers [15–16].

3. Results and discussion

3.1. Effect of BaO and MgO on contact angle

The wetting behaviors of the CaO–Al₂O₃-based mold fluxes on the IF steel substrates at 1773 K are shown in Fig. 3. All the flux samples on the top of the substrate transformed from original solid cubes into molten spherical caps due to the high temperature and surface shrinkage. The high temperature melts the mold fluxes and makes them flowable, but the surface shrinkage avoids being flattened due to the surface tension. The spherical cap shape of the mold flux also indicates that the wettability of the mold fluxes on the IF steel is not good, compared with that of the oxide inclusions on the alloy steel substrates, as our previous studies [14,17–18].
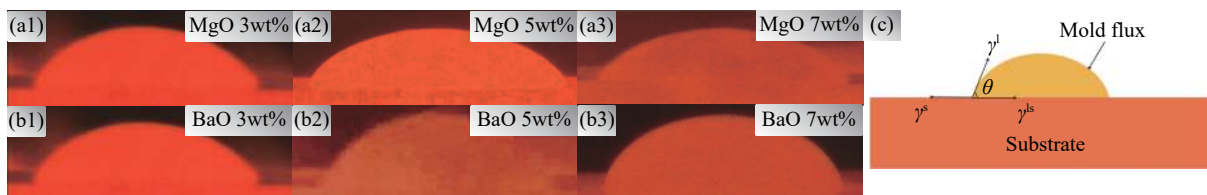

Fig. 3.   Wetting behavior of the mold fluxes with various BaO and MgO contents on the IF steel substrate: (a1–a3) MgO contents of 3wt%, 5wt%, and 7wt%, respectively; (b1–b3) BaO contents of 3wt%, 5wt%, and 7wt%, respectively; (c) measurement of the contact angle for Yong's equation.

Fig. 4 shows the change of the contact angle between the IF steel substrate and the CaO–Al₂O₃-based mold fluxes with various BaO and MgO contents. The contact angle increases from 62.4° to 74.5° with the increase of BaO content from 3wt% to 7wt%, which suggests that the addition of BaO can weak the wettability of mold flux on the IF steel. However, the contact angle decreases from 62.4° to 51.3° with the increase of MgO content from 3wt% to 7wt% at the same experimental conditions, so the MgO enhances the wettability and makes the mold flux spreading on the surface of IF steel more easily.

3.2. Effect of BaO and MgO on interfacial tension

The interfacial tension between the CaO–Al₂O₃-based

mold fluxes and the IF steel substrates was calculated using Young's equation (Eq. (1)) based on the measurement of contact angle (Fig. 4) from the sessile drop test as shown in Fig. 3(c).

$$\gamma^{ls} = \gamma^{s} - \gamma^{l}\cos\theta \qquad (1)$$

where γ^{s} is the surface tension of the IF steel; γ^{l} is the surface tension of the molten flux; γ^{ls} is the interfacial tension between them; θ is the contact angle.

The surface tension of IF steel (γ^{s}) was calculated from Eq. (2), which is the formula of surface tension of Fe as suggested by Brooks *et al.* [19]. The influence of alloy components on the surface tension of the substrate was ignored since the substrates are made of IF steel, and they contain very little
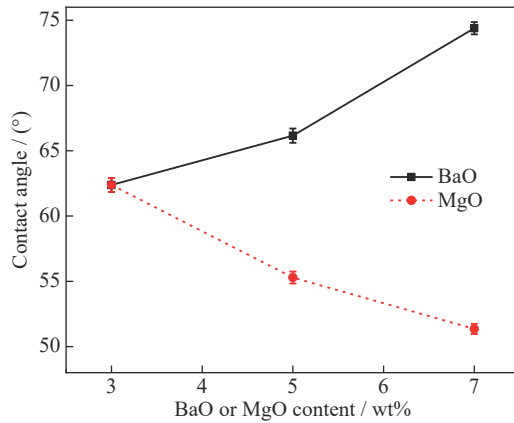
1182

Int. J. Miner. Metall. Mater., Vol. 29, No. 6, Jun. 2022

Fig. 4.   Contact angles at the interface between the IF steel substrate and the CaO–Al$_2$O$_3$-based mold fluxes with various BaO and MgO contents at 1773 K.

Table 3.   Surface tension factor of some pure substances [20–22]

Oxide	Surface tension factors / (mN·m^{-1})
CaO	$791 - 0.0935T$
SiO$_2$	$243.2 + 0.031T$
Al$_2$O$_3$	$1024 - 0.177T$
Na$_2$O	$438 - 0.116T$
Li$_2$O	$300 - 0.11T$
CaF$_2$	$1604.6 - 0.72T$
BaO	560 (1773 K)
MgO	$1770 - 0.636T$

alloys as listed in Table 2.

$$\gamma^s = 1870 - (T - 1811) \tag{2}$$

where T is the temperature (K), which should be in the range of 1740–1920 K.

The surface tension of the molten mold flux (γ^l) was obtained based on a partial molar approach, called as Boni's empirical equation [12].

$$\gamma^l = \sum \gamma_i \cdot N_i \tag{3}$$

where γ_i is the surface tension factor of a pure substance i; N_i is the molar fraction of the pure substance i as a component of the mold flux. The surface tension factors of these pure substances are listed in Table 3 [20–22].

Fig. 5 shows the calculated results of the interfacial tensions between the CaO–Al$_2$O$_3$-based mold fluxes and the IF steel substrates. The interfacial tension increases from 1630.3 to 1740.8 mN/m when the BaO content increases from 3wt% to 7wt%, as shown in Fig. 5(a). The increase of interfacial tension also indicates that the wettability of molten flux on the IF steel substrate gets weaker when BaO is added into the mold flux. The larger interfacial tension and weaker wettability due to the addition of BaO are beneficial for avoiding the capture of mold flux by the hooks on the solidified shell in continuous casting mold. In addition, the interfacial tension reduces from 1630.3 to 1539.7 mN/m with the increase of MgO content also from 3wt% to 7wt%, as shown in Fig.
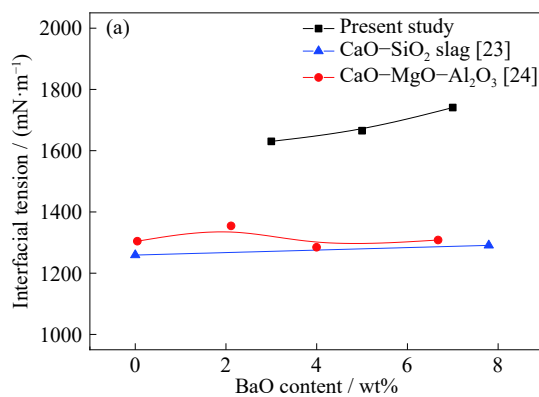
5(b). Therefore, the mold flux with the addition of MgO can make it easier to wet the solidified shell and be captured by the hooks, which may cause more slag inclusion defects in the casting product. The variation trends obtained here are consistent with the results from other researchers [23–26]. Of cause, the interfacial tensions in this study are relatively larger than others, which is reasonable since the compositions of slags and steels are different, and their experimental temperatures are also higher.

3.3. Effect of BaO and MgO on the oxygen species at the interface

The oxygen species at the interface between the CaO–Al$_2$O$_3$-based mold fluxes and the IF steel substrates have a great impact on wettability and interfacial tension [27–28]. Considering XPS is an effective surface analysis technology that can qualitatively and quantitatively analyze the elements and their chemical states on the surface of materials, the oxygen species at the interface between the mold flux and steel substrate were identified by XPS. Fig. 6(a) and (b) show the O 1s XPS spectra of the mold fluxes with different BaO and MgO contents, respectively. All the spectra has a big peak located at binding energy from about 533 to 529 eV.

Fig. 7 shows the deconvoluted peaks of bridging oxygen (O^0), non-bridging oxygen (O$^-$), and free oxygen (O^{2-}) as a function of binding energy. The fitting of these peaks were carried out by the Gaussian deconvolution with the coefficient of determination (R^2) above 99.7%. The specific positions of binding energies of O^0, O$^-$, and O^{2-} are around 532.16, 531.22, and 530.08 eV, and the optimum full width
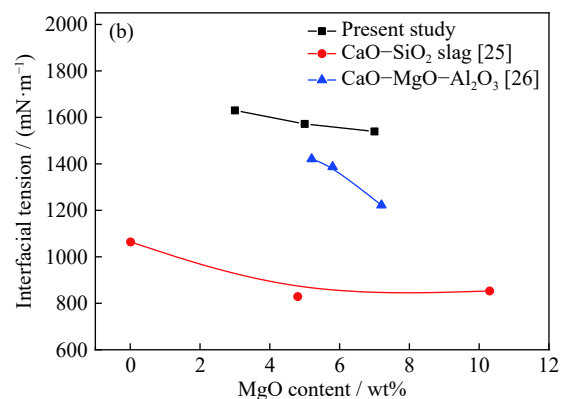

Fig. 5.   Interfacial tension between the IF steel substrate and mold fluxes with different contents of (a) BaO and (b) MgO.
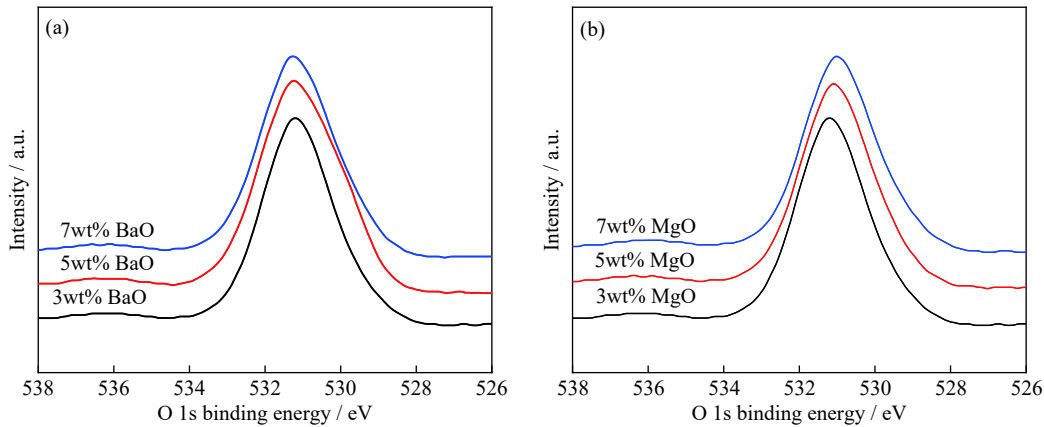
Fig. 6.   XPS spectra results of the mold flux with various (a) BaO content; (b) MgO content.
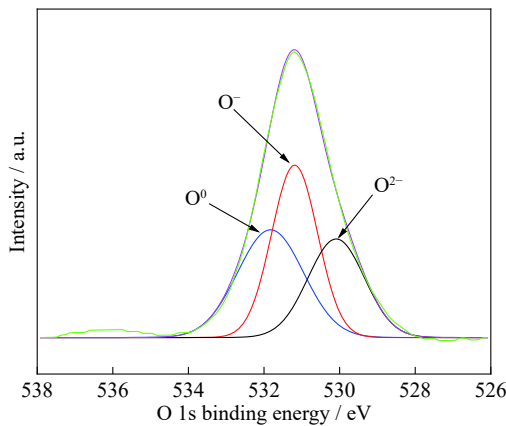

Fig. 7.   Typical deconvoluted XPS spectra of the mold fluxes sample 1.

at half maximum (FWHM) of the peaks on all the spectra are less than 2.0 eV. These results are listed in Table 4, which are consistent with previous studies [29–30].

The fractions of each oxygen species at the interface were obtained by calculating the integrated area of the deconvoluted peaks in Fig. 7. The variations of fractions of O^0, O$^-$, and O^{2-} with different BaO and MgO contents are shown in
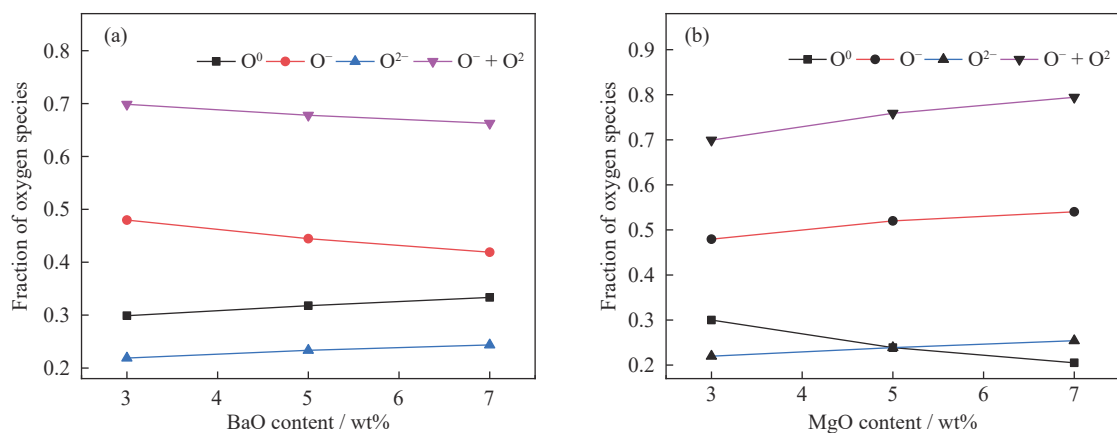
Table 4.   Peak analysis of O 1s in the designed mold flux system [29–30]

Sample	Binding energy / eV			FWHM / eV		
	O^{2-}	O$^-$	O^0	O^{2-}	O$^-$	O^0
1	530.08	531.22	532.16	1.94	1.66	1.98
2	530.03	531.19	532.07	1.81	1.67	1.95
3	530.01	531.16	532.03	1.78	1.73	1.96
4	530.15	531.22	531.97	1.92	1.65	1.93
5	530.13	531.33	532.56	1.98	1.71	1.92

Fig. 8. It can be found from Fig. 8(a) that the fraction of O$^-$+O^{2-} decreases, while that of O^0 increases with the addition of BaO. This tendency suggests that the melt structures of aluminate and silicate at the interface between molten flux and steel substrate are polymerized after adding BaO, since more non-bridging oxygen and free oxygen ions transformed into bridged oxygen. But, in Fig. 8(b), the fraction of O$^-$+O^{2-} increases, meantime that of O^0 decreases when MgO was added in the mold flux. The melt structures at the interface are depolymerized by the addition of MgO because some bridged oxygen is broken into non-bridging oxygen and free oxygen ions.

Fig. 8.   Fraction of O^{2-}, O$^-$, and O^0 in the CaO–Al$_2$O$_3$-based mold fluxes with various (a) BaO content and (b) MgO content at 1773 K.

Therefore, BaO and MgO work different on the melt structure at the interface between the CaO–Al$_2$O$_3$-based mold fluxes and the IF steel substrate, although they are all of alkaline earth metal oxides. Generally, alkaline metal and al-

kaline earth oxides work as network breakers in the silicate melt since they can offer O^{2-} to break the Si–O–Si into Si–O$^-$, sequentially, simplifies the melt structure [31–32]. However, it can be different in aluminate and aluminosilicate, as Ba^{2+}

1184

Int. J. Miner. Metall. Mater., Vol. 29, No. 6, Jun. 2022

and Mg^{2+} cations can embed into the $[AlO_4]^{5-}$ and Al–O–Si structural units to compensate the charge mismatching [33–34]. The charge compensation effect makes the structural units more stable and the melt structure more complex. So, whether BaO and MgO work as network breaker or former that is mainly depending on the comprehensive effects of offering O^{2-} and the charge compensation.

Specifically, in this study, the main reason why MgO works as network breaker, while BaO works as network former is that the charge compensation effect of Mg^{2+} is much smaller than Ba^{2+}. The ionic radius of Mg^{2+} cation is smaller than Ba^{2+} cation, and the electrostatic potential of Mg^{2+} is also higher [35]. The higher electrostatic potential leads to a strong polarization effect between O^{2-} and Mg^{2+}, which results in the transition of Mg–O bond from the ionic to the covalent in the molten mold flux. Consequently, the charge compensation effect of Mg^{2+} is weaken, and MgO plays the major role of releasing O^{2-} to depolymerize the network structure. However, the charge compensation effect of BaO is so strong that it offset the effect of providing O^{2-} and polymerizes the network structure.

In addition, based on the theory of Gibbs adsorption isotherm, the relationship between oxygen activity and interface interfacial tension can be expressed as Eq. (4) [27,30]:

$$\Gamma = -\frac{1}{RT} \cdot \frac{d\gamma^{ls}}{d(\ln a_O)} \approx -\frac{1}{RT} \cdot \frac{d\gamma^{ls}}{d(\ln X_O)} \quad (4)$$

where Γ is the saturation coverage; T is the temperature (K); R is the ideal gas constant (8.314 J·mol^{-1}·K^{-1}); a_O and X_O are the activity and the mole fraction of oxygen at the interface. In this study, the non-bridging oxygen (O$^-$) and free oxygen (O^{2-}) at the interface are regarded as solute, so $X_O = X_{O^-} + X_{O^{2-}}$.

Fig. 9 shows the variation of interfacial tension between mold flux and IF steel substrate at 1773 K with the change of $\lg(X_{O^-} + X_{O^{2-}})$. The slopes of both fitting lines are smaller than 0, which means saturation coverage (Γ) is positive. Therefore, the adsorption process that the migration of non-bridging oxygen and free oxygen from the bulk to the interface is a positive adsorption. Furthermore, the slopes of the two fitting lines are also different. This different mainly results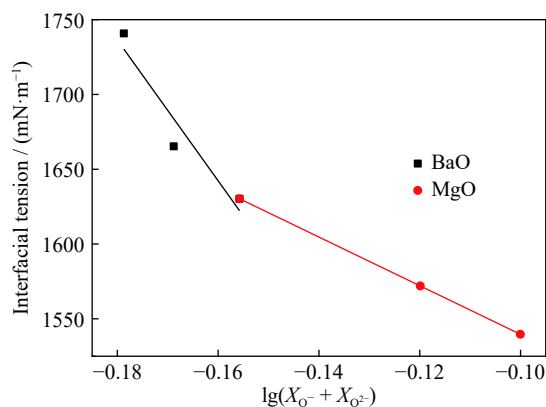 from the characteristics of the cations, since the electro-static potential of Mg^{2+} is larger than that of Ba^{2+}.

4. Conclusions

The effects of BaO and MgO contents on the wetting behavior of the CaO–Al$_2$O$_3$-based mold flux on IF steel substrate were investigated using sessile drop method. The oxygen species at the interface were determined using XPS. Some important conclusions were summarized as following.

(1) The contact angle increased from 62.4° to 74.5° with the increase of BaO content from 3wt% to 7wt%, while it decreased from 62.4° to 51.3° with the increase of MgO content from 3wt% and 7wt%. These trends suggested that BaO can weak the wettability, but MgO showed the opposite impact and enhanced the wettability of mold flux on the IF steel.

(2) The variation trends of interfacial tension with the BaO and MgO contents were consistent with that of contact angle. It increased from 1630.3 to 1740.8 mN/m when the BaO content increased from 3wt% to 7wt%, and reduced from 1630.3 to 1539.7 mN/m with the addition of MgO content also from 3wt% to 7wt%.

(3) The fraction of O$^-$+O^{2-} at the interface between molten flux and IF steel substrate decreased, while that of O^0 increased with the addition of BaO. On the contrary, the fraction of O$^-$+O^{2-} increased, meantime that of O^0 decreased when MgO was added in the mold flux. The main reason for that is because the charge compensation effect of BaO is stronger than MgO.

(4) The adsorption process of non-bridging oxygen (O$^-$) and free oxygen (O^{2-}) from the bulk to the interface was a positive adsorption, since the slopes of both fitting lines of γ^{ls} versus $\lg(X_{O^-} + X_{O^{2-}})$ were smaller than 0.

Acknowledgements

Conflict of Interest

Authors declare no potential conflict of interest.

References

[1] J. Yang, J.Q. Zhang, O. Ostrovski, C. Zhang, and D.X. Cai, Effects of B$_2$O$_3$ on crystallization, structure, and heat transfer of CaO–Al$_2$O$_3$-based mold fluxes, *Metall. Mater. Trans. B*, 50(2019), No. 1, p. 291.

[2] C.B. Shi, M.D. Seo, J.W. Cho, and S.H. Kim, Crystallization characteristics of CaO–Al$_2$O$_3$-based mold flux and their effects on in-mold performance during high-aluminum TRIP steels continuous casting, *Metall. Mater. Trans. B*, 45(2014), No. 3, p. 1081.

[3] Z.Y. Cai, B. Song, L.F. Li, Z. Liu, and X.K. Cui, Effect of

Fig. 9.   Effect of O$^-$+O^{2-} on the interfacial tension between mold flux and IF steel substrate.

CeO$_2$ on heat transfer and crystallization behavior of rare earth alloy steel mold fluxes, *Int. J. Miner. Metall. Mater.*, 26(2019), No. 5, p. 565.

[4] J. Yang, H.J. Cui, J.Q. Zhang, O. Ostrovski, C. Zhang, and D.X. Cai, Interfacial reaction between high-Al steel and CaO–Al$_2$O$_3$-based mold fluxes with different CaO/Al$_2$O$_3$ ratios at 1773 K (1500°C), *Metall. Mater. Trans. B*, 50(2019), No. 6, p. 2636.

[5] Y. Nakamura, T. Ando, K. Kurata, and M. Ikeda, Effect of chemical composition of mold powder on the erosion of submerged nozzles for continuous casting of steel, *Trans. Iron Steel Inst. Jpn.*, 26(1986), No. 12, p. 1052.

[6] J. Yang, J.Q. Zhang, O. Ostrovski, Y. Sasaki, C. Zhang, and D.X. Cai, Dynamic wetting of high-Al steel by CaO–SiO$_2$- and CaO–Al$_2$O$_3$-based mold fluxes, *Metall. Mater. Trans. B*, 50(2019), No. 5, p. 2175.

[7] P. Fei, Y. Min, C.J. Liu, and M.F. Jiang, Effect of continuous casting speed on mold surface flow and the related near-surface distribution of non-metallic inclusions, *Int. J. Miner. Metall. Mater.*, 26(2019), No. 2, p. 186.

[8] L.J. Zhou, Z.H. Pan, W.L. Wang, and J.Y. Chen, Study of the Ni–Cr–Fe-based alloy casting process using a mold simulator technique, *Steel Res. Int.*, 91(2020), No. 3, art. No. 1900503.

[9] A. Sharan and A.W. Cramb, Surface tension and wettability studies of liquid Fe–Ni–O alloys, *Metall. Mater. Trans. B*, 28(1997), No. 3, p. 465.

[10] J. Lee and K. Morita, Evaluation of surface tension and adsorption for liquid Fe–S alloys, *ISIJ Int.*, 42(2002), No. 6, p. 588.

[11] K. Nakashima and K. Mori, Interfacial properties of liquid iron alloys and liquid slags relating to iron- and steel-making processes, *ISIJ Int.*, 32(1992), No. 1, p. 11.

[12] E.J. Jung, W. Kim, I. Sohn, and D.J. Min, A study on the interfacial tension between solid iron and CaO–SiO$_2$–MO system, *J. Mater. Sci.*, 45(2010), No. 8, p. 2023.

[13] W.L. Wang, J.W. Li, L.J. Zhou, and J. Yang, Effect of MnO content on the interfacial property of mold flux and steel, *Met. Mater. Int.*, 22(2016), No. 4, p. 700.

[14] L.J. Zhou, J.W. Li, W.L. Wang, and I. Sohn, Wetting behavior of mold flux droplet on steel substrate with or without interfacial reaction, *Metall. Mater. Trans. B*, 48(2017), No. 4, p. 1943.

[15] W.L. Wang, H.Q. Shao, L.J. Zhou, H. Luo, and H.F. Wu, Rheological behavior of the CaO–Al$_2$O$_3$-based mold fluxes with different Na$_2$O contents, *Ceram. Int.*, 46(2020), No. 17, p. 26880.

[16] W.L. Wang, S.F. Dai, L.J. Zhou, J.K. Zhang, W.G. Tian, and J.L. Xu, Viscosity and structure of MgO–SiO$_2$-based slag melt with varying B$_2$O$_3$ content, *Ceram. Int.*, 46(2020), No. 3, p. 3631.

[17] L.J. Zhou, Z.H. Pan, W.L. Wang, and J.Y. Chen, Optimization of the interfacial properties between mold flux and TiN substrate through the regulation of B$_2$O$_3$, *ISIJ Int.*, 60(2020), No. 12, p. 2838.

[18] L.J. Zhou, Z.H. Pan, W.L. Wang, J.Y. Chen, L.W. Xue, T.S. Zhang, and L. Zhang, Interfacial interactions between inclusions comprising TiO$_2$ or TiN and the mold flux during the casting of titanium-stabilized stainless steel, *Metall. Mater. Trans. B*, 51(2020), No. 1, p. 85.

[19] R. Brooks, I. Egry, S. Seetharaman, and D. Grant, Reliable data for high-temperature viscosity and surface tension: Results from

a European project, *High Temp.-High Pressures*, 33(2001), No. 6, p. 631.

[20] M. Hanao, T. Tanaka, M. Kawamoto, and K. Takatani, Evaluation of surface tension of molten slag in multi-component systems, *ISIJ Int.*, 47(2007), No. 7, p. 935.

[21] K.C. Mills, L. Yuan, and R.T. Jones, Estimating the physical properties of slags, *J. South. Afr. Inst. Min. Metall.*, 111(2011), No. 10, p. 649.

[22] K.C. Mills, S. Karagadde, P.D. Lee, L. Yuan, and F. Shahbazian, Calculation of physical properties for use in models of continuous casting process-Part 1: Mould slags, *ISIJ Int.*, 56(2016), No. 2, p. 264.

[23] H.P. Sun, K. Nakashima, and K. Mori, Influence of slag composition on slag–iron interfacial tension, *ISIJ Int.*, 46(2006), No. 3, p. 407.

[24] K. Ogino, Interfacial tension between molten iron alloys and molten slags, *Tetsu-to-Hagane*, 61(1975), No. 8, p. 2118.

[25] S.C. Park, H. Gaye, and H.G. Lee, Interfacial tension between molten iron and CaO–SiO$_2$–MgO–Al$_2$O$_3$–FeO slag system, *Ironmaking Steelmaking*, 36(2009), No. 1, p. 3.

[26] R. Hagemann, H.P. Heller, S. Lachmann, S. Seetharaman, and P.R. Scheller, Slag entrainment in continuous casting and effect of interfacial tension, *Ironmaking Steelmaking*, 39(2012), No. 7, p. 508.

[27] E.J. Jung and D.J. Min, Effect of Al$_2$O$_3$ and MgO on interfacial tension between calcium silicate-based melts and a solid steel substrate, *Steel Res. Int.*, 83(2012), No. 7, p. 705.

[28] J.B. Kim, J.K. Choi, I.W. Han, and I. Sohn, High-temperature wettability and structure of the TiO$_2$–MnO–SiO$_2$–Al$_2$O$_3$ welding flux system, *J. Non-Cryst. Solids*, 432(2016), p. 218.

[29] L.J. Zhou, H. Li, W.L. Wang, D. Xiao, L. Zhang, and J. Yu, Effect of Li$_2$O on the behavior of melting, crystallization, and structure for CaO–Al$_2$O$_3$-based mold fluxes, *Metall. Mater. Trans. B*, 49(2018), No. 5, p. 2232.

[30] W.L. Wang, E.Z. Gao, L.J. Zhou, L. Zhang, and H. Li, Effect of Al$_2$O$_3$/SiO$_2$ and CaO/Al$_2$O$_3$ ratios on wettability and structure of CaO–SiO$_2$–Al$_2$O$_3$-based mold flux system, *J. Iron. Steel Res. Int.*, 26(2019), No. 4, p. 355.

[31] H.Y. Yu, X.L. Pan, Y.P. Tian, and G.F. Tu, Mineral transition and formation mechanism of calcium aluminate compounds in CaO–Al$_2$O$_3$–Na$_2$O system during high-temperature sintering, *Int. J. Miner. Metall. Mater.*, 27(2020), No. 7, p. 924.

[32] J.Y. Chen, W.L. Wang, L.J. Zhou, and Z.H. Pan, Effect of Al$_2$O$_3$ and MgO on crystallization and structure of CaO–SiO$_2$–B$_2$O$_3$-based fluorine-free mold flux, *J. Iron Steel Res. Int.*, 28(2021), No. 5, p. 552.

[33] E.Z. Gao, W.L. Wang, and L. Zhang, Effect of alkaline earth metal oxides on the viscosity and structure of the CaO–Al$_2$O$_3$ based mold flux for casting high-al steels, *J. Non-Cryst. Solids*, 473(2017), p. 79.

[34] G.H. Zhang, K.C. Chou, and K. Mills, Modelling viscosities of CaO–MgO–Al$_2$O$_3$–SiO$_2$ molten slags, *ISIJ Int.*, 52(2012), No. 3, p. 355.

[35] J.A. Duffy and M.D. Ingram, Optical basicity—IV: Influence of electronegativity on the Lewis basicity and solvent properties of molten oxyanion salts and glasses, *J. Inorg. Nucl. Chem.*, 37(1975), No. 5, p. 1203.